ELSEVIER

Contents lists available at ScienceDirect

Chemical Engineering Journal

journal homepage: www.elsevier.com/locate/cej





HZSM-5 supported with N-doped Fe for microwave catalytic pyrolysis of lignin

Yan Wang ^a, Kangqi Cao ^a, Wenlong Sun ^a, Xiangxi Lin ^a, Jianwei Wang ^b, Jessica Villarreal ^c, Longzhi Li ^a, ^{*}

- a College of Mechanical and Electronic Engineering, Shandong University of Science and Technology, 266590 Qingdao, Shandong Province, China
- b College of Energy Storage Technology, Shandong University of Science and Technology, 266590 Qingdao, Shandong Province, China
- ^c Department of Chemistry and Physics, College of Science, The University of Texas Permian Basin, 79762 Odessa, TX, USA

ARTICLE INFO

Keywords: Microwave catalytic pyrolysis Lignin N-doped Fe HZSM-5

ABSTRACT

Microwave catalytic pyrolysis of lignin is one of emerging technologies for efficiently converting lignin into fuels and chemicals. Molecular sieves (HZSM-5) are widely used as carriers to load metallic components for biomass pyrolysis but often encounter challenges such as high diffusion resistance and insufficient acidity of acidic sites. Traditionally, HZSM-5 is directly modified to enhance the activity of the acidic sites, but this modification is ineffective in improving the metallic components' activity. Instead, we made nitrogen doping on Fe and then supported on HZSM-5 to construct Fe-N₂₅/HZSM-5 catalysts for microwave catalytic pyrolysis of lignin. The N-doped Fe has the effect of "killing two birds with one stone" on enhancing the catalytic activity. The characterization results indicated that N replaced C of the graphitic carbon network to form carbon nitride structure, and further combined with Fe to generate Fe-N bonds, improving the electronegativity of the metallic component. Besides, the loading of N-doped Fe increased the acidity of the catalyst. The utilization of 1.00Fe-N_{25} /HZSM-5 obtained the greatest bio-gas yield (35.2 wt%), a hydrogen yield of 27.8 mL/min, bio-oil yield (36.4 wt %) and phenol selectivity of 46.2 %. The likely pathway of microwave catalytic pyrolysis on Fe-N₂₅/HZSM-5 was proposed through DFT calculation, using guaiacol as a model compound. The results suggested that N-doped Fe on HZSM-5 8 T tended to break the side-chain methoxy during pyrolysis of guaiacol, with energy barrier of 0.14 eV. This paper provides a promising strategy for modification of microwave pyrolysis catalysts.

1. Introduction

Lignin as an abundant renewable aromatic polymer serves as one of the main components of biomass. It is primarily composed of three phenylpropane (C_9) basic structural units, including guaiacyl (G-type), syringyl (S-type), and p-hydroxyphenyl (H-type) [1,2]. Lignin possesses a complex cross-linking structure, making it difficult to convert into a higher-value precursor [3]. Pyrolysis is an effective method to convert lignin into high-value-added biofuels and chemical raw materials under anoxic conditions [4–6]. Conventional pyrolysis encounters some challenges, such as low efficiency, inadequate product selectivity, and excessive energy consumption, hindering efficient conversion of lignin [7]. The even heating peculiarity of microwaves and the directional convergence of energy enables microwave catalytic pyrolysis of lignin to achieve high reaction rates and product selectivity with reduced energy consumption [8–11]. Consequently, microwave pyrolysis of lignin is

considered to be an alternative to the conventional pyrolysis method. Xue et al. applied microwave systems to the catalytic dehydration of glycerol for the sustainable production of acrolein and showed that microwave heating was more efficient than electrical heating for the dehydration of glycerol to acrolein at lower temperature [12]. Zhou et al. found that catalytic pyrolysis of plastic waste in a continuous microwave-assisted pyrolysis system could produce higher-quality biooil and bio-char compared to conventional pyrolysis [13].

Currently, microwave catalytic pyrolysis of lignin has attracted a great deal of interests. The main challenges faced by microwave pyrolysis of lignin are to reduce the energy consumption of pyrolysis reaction as well as improve the yield and selectivity of pyrolysis products. For this purpose, the catalyst with high activity and stability is especially crucial, which can enhance the pyrolysis rate, improve the products distribution and selectivity with the help of persistent catalytic activity. The catalyst plays a significant role in determining the pyrolysis rate, product yield

E-mail address: lilongzhi630@163.com (L. Li).

^{*} Corresponding author.

and selectivity. Catalyst is generally loaded with metallic components using metal oxides, carbon and molecular sieves, and so on as carriers [14-16]. Hendry et al. investigated the effect of ZrO_2 loaded with different metals on the catalytic pyrolysis of lignin and found that Na/ ZrO_2 was effective in improving the product selectivity of bio-oil [17]. Huang et al. performed in-situ catalytic pyrolysis of lignin with Ga and Zr loaded on HZSM-5, and discovered that the catalysts promoted olefin aromatization [18].

Molecular sieves, as carriers, have good thermal stability and relatively low cost, are considered as one of the optimum catalyst carriers [19]. The molecular sieves primarily consist of HZSM-5, H-Ferrierite, H-Mordenite, H-Beta, and H-USY etc. [20]. HZSM-5 possess high silica-toaluminium ratio and a unique two-dimensional channel pore structure, as well tunable Lewis and Brønsted acid active sites, facilitating lignin chemical bond breaking [21-23]. However, as carrier, it is not very selective for the product. The metallic component can adsorb the reactant and form a synergistic effect with the carrier to increase catalyst activity, including non-precious metals (Cu, Fe, Co, etc.) and precious metals (e.g., Pt, Pd, Rh, Ru, etc.) [24,25]. Among them, Fe and Co are cheaper but less stable. Catalyst modification is an essential way to improve the catalytic activity of acid active sites of molecular sieves [26]. In previous studies, catalyst modification often focuses on the Ndoping of carriers and rarely puts the research perspective on the Ndoping of metallic components. Innovatively, the treatment of nitrogen doping on Fe was made to obtain the N-doped Fe for the subsequent catalyst preparation in this work. The N-doped metallic modification is due to higher electronegativity and more lone pair electrons of nitrogen, which can form new electronic states with the surface of metallic components and change the local electron density [27]. However, the intrinsic effect of N-doping on the modification of the metallic components, the overall catalyst activity and the mechanism of selective bond breaking under the loading of N-doped metallic components on HZSM-5 catalysts remains unclear. Regarding this fact, we paid attention to identify the mechanism of Fe-N $_{\rm 25}$ supported on HZSM-5 on the microwave catalytic pyrolysis of lignin through the experiments and simulations.

In this study, Fe-N $_{25}$ /HZSM-5 was prepared as co-catalyst based on "killing two birds with one stone" strategy, and lignin product distribution and its selectivity were investigated. The morphological characteristics of the catalysts were studied using various characterization techniques. The optimal catalytic pyrolysis pathway was explored using density-functional theory (DFT), using guaiacol as the lignin modeling compound, and the mechanism of selective bond breaking was investigated. This paper provides a good reference for preparing highly active lignin pyrolysis catalysts.

2. Experimental

2.1. Catalyst preparation and characterization

Alkaline lignin purchased from Shanghai Macklin Biochemical Co., Ltd was used for microwave catalytic pyrolysis. Before the pyrolysis, alkaline lignin was crushed and sieved to 100–120 mesh. The metallic salts (Fe(NO₃)₃-9H₂O, Co(NO₃)₃-5H₂O), nitrogen source (melamine) and HZSM-5 (SiO₂/Al₂O₃ = 25, crystallinity \geq 95 %) were purchased from Shanghai Aladdin Biochemical Technology Co., Ltd and used for catalyst preparation. Before the test, HZSM-5 was pre-treated by ball milling and the powder was collected over 80–100 mesh sieve.

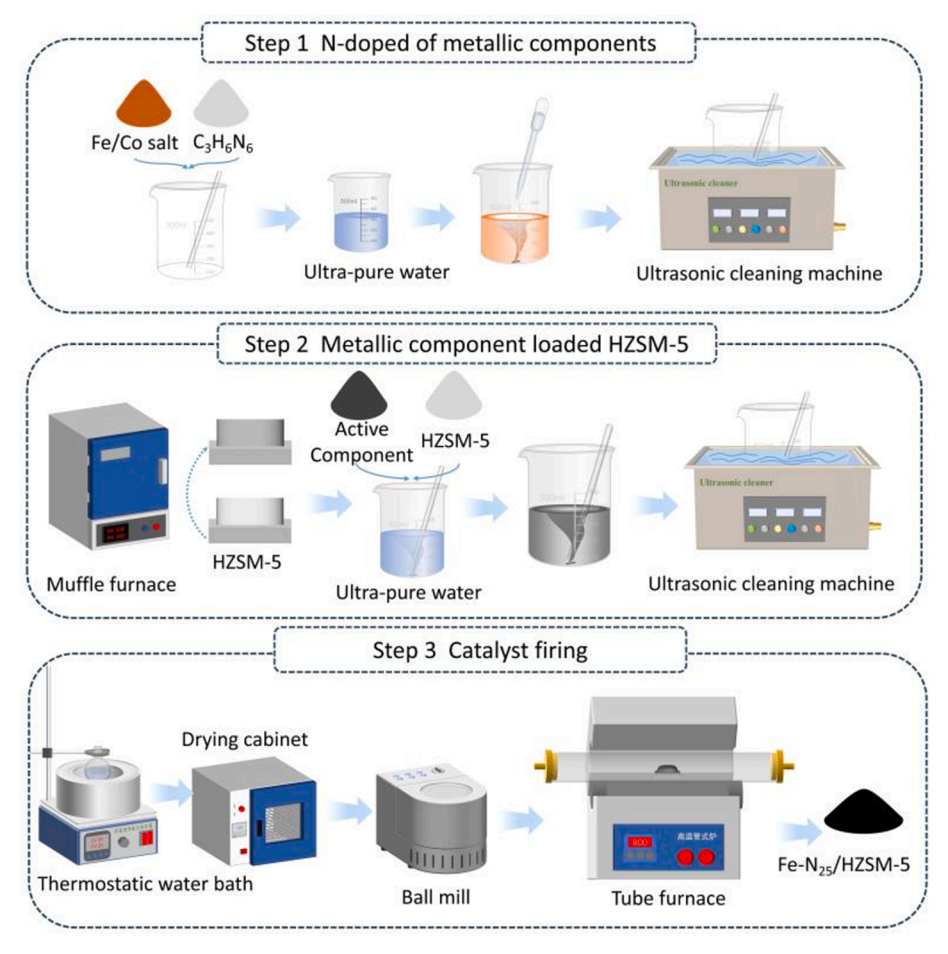


Fig. 1. Catalyst preparation process.

The catalyst preparation process was shown in Fig. 1. First, $C_3H_6N_6$ and $Fe(NO_3)_3\text{-}9H_2O$ solid powder were stirred evenly, and an ultrasonic treatment was performed for two hours. The powder was obtained by ball milling after drying in an oven at 100 $^{\circ}\text{C}$ for 12 h. It was placed in a tube furnace under an argon atmosphere and calcined according to the following procedure: the samples were heated up to 800 $^{\circ}\text{C}$ for two hours at a heating rate of 5 $^{\circ}\text{C/min}$ to obtain the N-doped metallic component named Fe-N₂₅.

HZSM-5 was calcined in a muffle furnace at 550 $^{\circ}$ C for five hours to remove internal impurities and template agent. Fe-N₂₅ and HZSM-5 were mixed thoroughly with ultrasonic treatment for two hours, and then stirred at a constant temperature of 85 $^{\circ}$ C to form a black powder. After drying, the catalyst was ball-milled into powder to obtain precursors finally calcined to obtain catalyst powders with different loading. The prepared catalysts were named 0.50Fe-N₂₅/HZSM-5, 0.75Fe-N₂₅/HZSM-5, and 1.00Fe-N₂₅/HZSM-5 based on the loading of 0.50 mmol/g, 0.75 mmol/g, 1 mmol/g, respectively.

The crystal structures and species of the catalysts were measured by an X-ray diffraction (XRD) analyzer (D8 Advance, Bruker), and was operated at the $2\theta^\circ$ range from 20 to 70° and with a scanning speed of 5° /min. X-ray photoelectron spectroscopy (XPS) was performed on a Thermo Scientific K-Alpha model instrument to determine the elemental composition and chemical state of the sample. The composition of pyrolytic oil was detected by gas chromatography-mass spectrometry (GC–MS, QP2020), and bio-gas were analyzed on a gas chromatograph (GC, TRACE 1310). The NH $_3$ temperature-programmed desorption (NH $_3$ -TPD) was obtained on a Micromeritics AutoChem 2920 instrument.

2.2. Microwave catalytic pyrolysis of lignin

Microwave catalytic pyrolysis of lignin was carried out in a Galanz domestic microwave oven (G80F20CN2L-B8), as shown in Fig. 2. The 0.3 g of catalyst and 1.5 g of lignin were mixed in a quartz reactor and purged with nitrogen for 10 min. The pyrolysis experiment was carried out at different microwave powers for 20 min. The gas flow rate of nitrogen was maintained at 200 mL/min during pyrolysis. The microwave thermogravimetric analyzer (MTGA, WSK12) was used to test the heating process and mass changes during the pyrolysis of lignin using different catalysts. Before the test, the catalyst and lignin were weighed according to a mass ratio of 1:5, and then the mixture was placed in a quartz crucible (Φ 42 mm \times 55 mm), which was completely sealed with a quartz lid. The quartz crucible was supported by a quartz tray and connected to an electronic balance that had an accuracy of 0.001 g. An infrared thermometer was utilized to measure the changes of bed temperature, whose temperature measurement range was 0–1000 °C. During the experiment, the flow rate of nitrogen was retained at 200 mL/min until the end of pyrolysis. Bio-gas are collected by an aluminum foil gas-collecting bag attached

to the end of the condensation system and was detected by gas chromatography (GC). Bio-oil was collected after extraction, filtration and spinning, and was detected by gas chromatography-gas chromatography-mass spectrometry (GC–MS). The solid products were measured on an electronic balance (HZK-FA2205). For each experiment, three replications were carried out and averaged the results.

The three-phase product yields of microwave catalytic pyrolysis of lignin were calculated according to Eqs. (1), (2) and (3):

$$Y_{\rm char} = \left(m_{\rm char}/m_{\rm Lignin}\right) \times 100\% \tag{1}$$

$$Y_{\rm oil} = \left(m_{\rm oil}/m_{\rm Lignin}\right) \times 100\% \tag{2}$$

$$Y_{\rm gas} = (m_{\rm gas}/m_{\rm Lignin}) \times 100\% \tag{3}$$

Bio-gas component volume fraction (Vol.%) and lower heating values were calculated according to equations (4) and (5):

$$V_{\rm X} = (A_{\rm X}/{\rm Atotal}) \times 100 \tag{4}$$

$$J_{\text{LHV}} = (12.64 \times V_{\text{CO}} + 10.79 \times V_{\text{H}_2} + 35.88 \times V_{\text{CH}_4}) \times 10^{-3}$$
 (5)

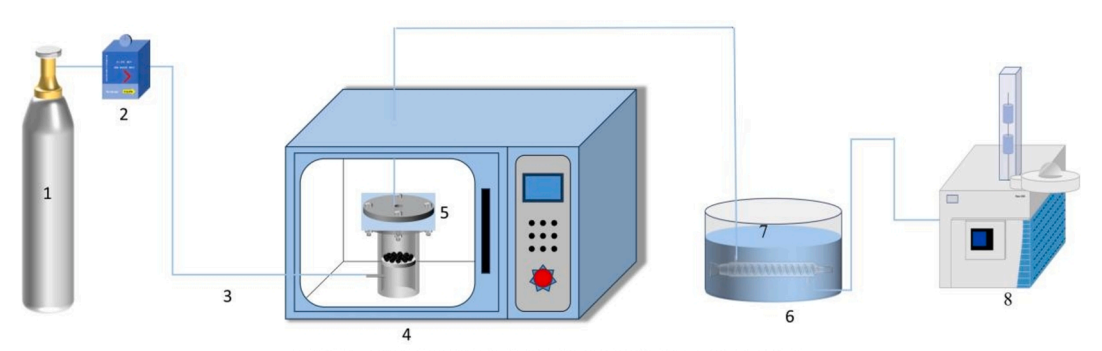
where $A_{\rm total}$ (Vol.%) is the sum of the relative peak areas of the bio-gas, and $J_{\rm LHV}$ (MJ/Nm³) is the low-level calorific value of the bio-gas, the subscripts $_{\rm X}$ denote the bio-gas CO $_{\rm 2}$, CO, CH $_{\rm 4}$ and H $_{\rm 2}$. The gas products like C $_{\rm 2}$ and C $_{\rm 3}$ hydrocarbons are almost no produced in the microwave catalytic pyrolysis of lignin. It was detected that the volume content of these gases are less than 0.5 %. Considering this fact, the other gas products are not taken into account for calculation of the total calorific value.

The relative content of each component in the liquid product was determined using a semi-quantitative method, i.e., the percentage area of the chromatographic peaks was calculated to determine the relative content of each component in the liquid product using the formula in (6):

$$S_{\rm aro} = \frac{I_{\rm aro}}{\sum I_{\rm aro}} \tag{6}$$

where $S_{\rm aro}$ (%) and $I_{\rm aro}$ (area.%) are the selectivity and peak area of each component, respectively, and $\sum I_{\rm aro}$ (area.%) is the total peak area of all components. Compound content is the percentage of all compounds determined by GC/MS, while selectivity indicates the percentage relative to a particular class of compounds.

After drying, bio-gas was analyzed for its component by gas chromatography, and the mass of bio-gas was calculated to obtain the gas yield. The mass of the quartz reactor before and after the pyrolysis reaction was weighed to determine the bio-char yield. The mass difference before and after the pyrolysis reaction is used by subtraction method to



Nitrogen cylinder; 2. Flow meter; 3. Ventilation tube; 4. Microwave oven;
 5. quartz reactor; 6. water sink; 7. Condenser; 8. gas chromatograph

Fig. 2. Microwave heat treatment device.

determine the mass of bio-oil, thereby establishing its yield.

2.3. Calculation method

GaussView 5.0 and Gaussian 09 W software were used to calculate the pathway of lignin pyrolysis in the presence of Fe-N₂₅/HZSM-5. To simplify the calculations, HZSM-5 T, 8 T and 8 T loaded clusters were established as catalyst models. The improved hybrid density functional M06-2X is used for calculations to geometrically optimize reactant, intermediate, transition state and product configurations to better describe weak interactions such as electronic correlations and van der Waals forces. The breakage of the phenyl side-chain bonds (R-O-R') is an effective depolymerization pathway to obtain aromatic monomers. Therefore guaiacol containing these key bridging bonds was selected as the lignin moulding compound. Different N-C species with or without metal embedding were used as adsorption substrates to explore the

effect of different substrates on molding in pyrolysis. The adsorption studies of lignin model compounds were also carried out using different molecular sieve cluster models. Employing the electrostatic potential further describes the nature and behavior of the electric field resulting from the distribution of charges in space, and is used to explain the interactions between molecular sites, the formation of electric fields, and changes in the potential energy. To explore the effect of loading of N-doped metallic components on the active site on HZSM-5. The potential pyrolysis pathway was explored by calculating the transition states and reaction energy barriers during lignin bond breaking. The aim was to illustrate the selectivity and stability of Fe-N $_{\rm 25}/\rm HZSM-5$ for microwave catalytic pyrolysis of lignin.

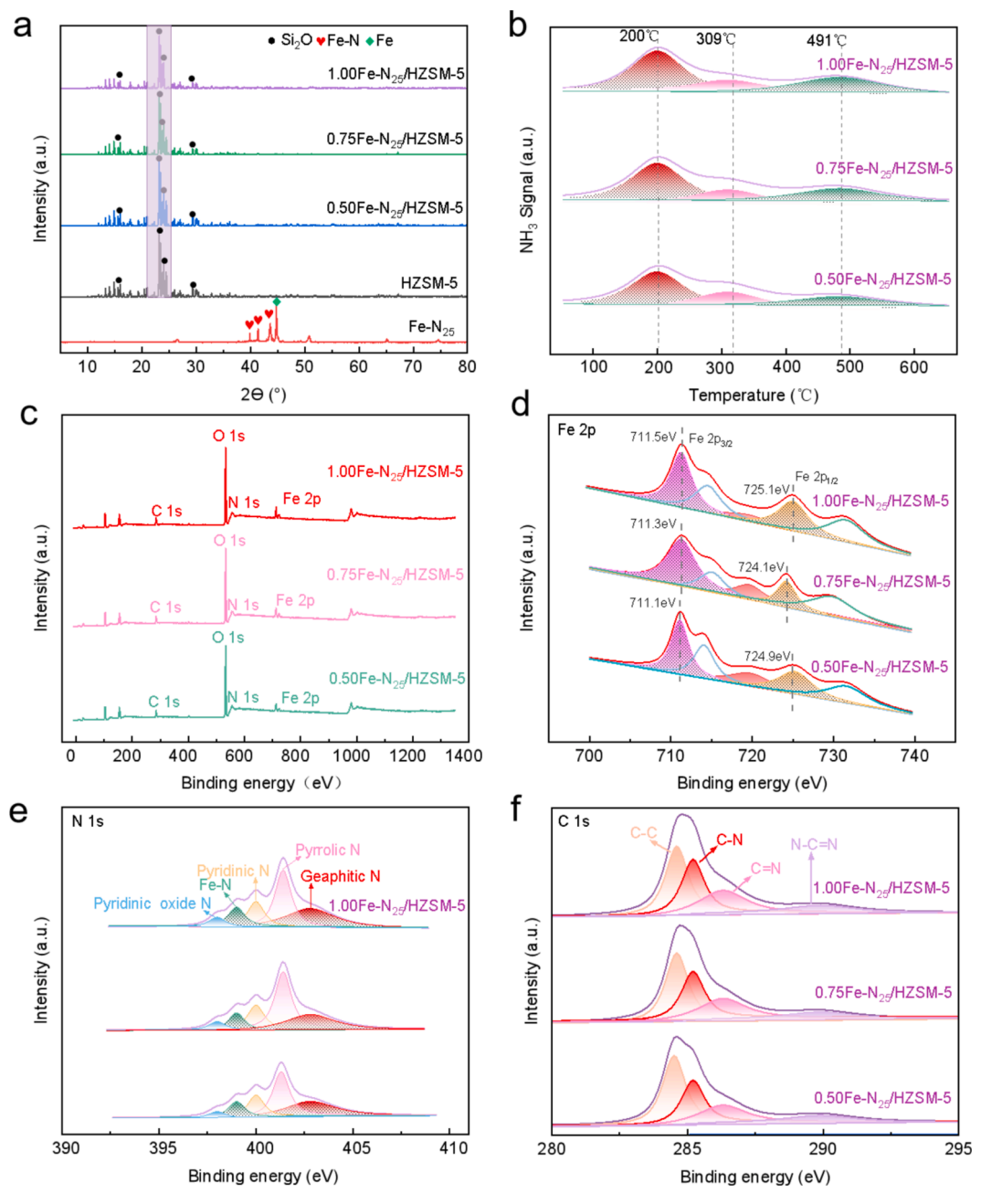


Fig. 3. Characterization of catalysts. a. XRD; b·NH₃-TPD; c-f. XPS.

3. Results and discussion

3.1. Catalyst characterization

In order to study the effect of N-doped Fe on the catalyst crystals, the catalysts were characterized by XRD (Fig. 3a). The characteristic peak of Fe-N and Fe appear at 38.2° and 43.8° for the metallic component, respectively. In contrast, the Fe-N and Fe characteristic peaks were not detected in the Fe-N25/HZSM-5 spectra. The crystallized MFI characteristic peaks of HZSM-5 was shown by the highlighted area in the picture, which appeared at the ranges of $12.0^{\circ} \sim 18.0^{\circ}$ and $22.5^{\circ} \sim 37.0^{\circ}$. This indicated that the metallic components were well dispersed on HZSM-5 and without destroying the MFI topographic structure of HZSM-5 [28]. To further investigate the effect of metallic components on the acidic sites of HZSM-5, the catalyst was tested for NH₃-TPD. As shown in Fig. 3b, three characteristic NH₃ desorption peaks appeared at 202 °C, 309 °C and 498 °C, which can be described as weak acidic site (202 °C), medium acidic site (309 °C), and strong acidic site (498 °C), respectively [29]. With the increase of metallic components loading, the peak area of weak and strong acid regions became larger, and the medium acid region became smaller, where 1.00Fe-N₂₅/HZSM-5 peak area became more prominent in the weak acid region, and the medium acid was shifted to the strong acid region. The order of magnitude of total acidity for different catalysts is 1.00Fe-N₂₅/HZSM-5 > 0.75Fe-N₂₅/HZSM-5 >0.50Fe-N₂₅/HZSM-5. It is suggested that higher loading of metallic components makes Fe-N₂₅/HZSM-5 more acidic. The catalysts were further analyzed by XPS (Fig. 3c, d, e, and f). It is observed in Fig. 3d that two major Fe 2p peaks centered at 711 eV and 725 eV in the highresolution energy spectrum of Fe-N25/HZSM-5 Fe 2p, which corresponded to Fe $2p_{3/2}$ and Fe $2p_{1/2}$ [29]. Interestingly, the overall peak intensity for 1.00Fe-N25/HZSM-5 is much higher than that of 0.50Fe- $N_{25}/HZSM$ -5 and 0.75Fe- $N_{25}/HZSM$ -5. This result indicates that the metallic components are well dispersed in HZSM-5, which is consistent with the XRD analysis results. As illustrated in Fig. 3e, the different N species can be distinguished according to the binding energy about 398.2 eV, 399.3 eV, 400.3 eV, 401.5 eV, and 402.8 eV, which are assigned to pyridinic-N-oxidation, Fe-N, pyridinic-N, pyrrolic-N, and graphitic-N, respectively. Among them, the peak area of pyrrolic-N is the most prominent, indicating that the N element in the catalyst mainly exists in the form of pyrrolic-N. Pyrrolic-N is mainly present in the defective structure of the carrier, coordinating with Fe through the Fe-N bonds and enhancing the dispersion of metallic components. Fig. 3f illustrated the high-resolution C 1s spectrum of the catalyst with four peaks corresponding to N-C = N (298.7 eV), C = N (286.5 eV), C-N (284.9 eV), and C-C (284.0 eV), indicating that some of the N replaced C of graphitic carbon network to form a carbon nitride structure in the Ndoping process, which again proves that the N-doped Fe on HZSM-5 was successfully synthesized [30].

3.2. Microwave-assisted pyrolysis using Fe-N₂₅/HZSM-5

3.2.1. Product distribution

Fig. 4a and b show the bed warming curves and weight loss characteristics for different catalysts mixed with lignin at microwave power of 700 W. As can be seen in Fig. 4a, the final temperature of $1.00 \, \text{Fe-N}_{25}/\text{HZSM-5}$ was as high as 598.1 °C, significantly higher than that of the other catalysts, and the pyrolysis ended 30 s earlier. Due to the poor wave-absorbing property of lignin in the absence of a catalyst, the bed temperature rose to the highest value of $598.1 \,^{\circ}\text{C}$ until $350 \, \text{s}$. The weight loss curve in Fig. 4b revealed that the pyrolysis in the presence of HZSM-5 continued until the end of $431 \, \text{s}$, and the final weight loss remained at $46.49 \, \text{wt}\%$. This is because HZSM-5 is mainly composed of silicaluminate, and the low magnetic loss coefficient leads to the difficulty of converting microwaves into heat so the lignin cannot be sufficiently pyrolyzed. When the N-doped Fe was loaded, the catalysts had a higher relative dielectric constant than that of HZSM-5, resulting in excellent

microwave absorption, and the pyrolysis stage was advanced to end at 280 s. Correspondingly, the final weight loss reduced to 44.63 wt%, 42.58 wt% and 42.61 wt% for 0.50 Fe-N $_{25}$ /HZSM-5, 0.75 Fe-N $_{25}$ /HZSM-5, and 1.00 Fe-N $_{25}$ /HZSM-5. The reason behind this is that the addition of a catalyst promotes the rapid conversion of microwaves into heat, allowing pyrolysis to proceed quickly.

The three-phase product yields of lignin pyrolysis are indicated in Fig. 4c. The addition of the catalyst produces more bio-oil and significantly less bio-char. This is caused by the ability of the Fe site in the metallic component to adsorb and activate electron pairs and N provides lone-pair electrons that exhibit acidic properties, forming the active site of Lewis and Brønsted acids [31–33]. The increased active site promotes selective bond breaking in the lignin unit structure. The bio-oil decreases with increasing N-doped Fe, this is attributed to some aromatic hydrocarbons is further converted into bio-gas with the enhancement of bed temperature. Distribution of biogas, as seen in Fig. 4d. CO₂ is the main component of biogas without a catalyst, and H2 becomes the main component when the catalyst is added. As the N-doped Fe increases, the volume fraction of CH₄ increases gradually. This is because the increased active sites of the catalyst promotes the removal of hydroxyl and methyl groups from the side chain moiety to produce CH₄. Fig. 4e shows the variation curves of calorific value and hydrogen production rate. The addition of the catalyst increased the calorific value from 6.41 MJ/Nm³ without a catalyst to 15.12 MJ/Nm³ in the presence of 1.00 Fe-N₂₅/HZSM-5. This is due to the increase of metallic component loading, the methane and syngas content increases and the calorific value becomes larger. The hydrogen production rate becomes larger with the increase of metallic component loading, which is caused by the fact that the loading of metallic components promotes the breakage of hydrogencontaining groups in the side chains of pyrolysis products to generate

The bio-oil was analyzed by GC/MS, which mainly consisted of aromatic compounds (thick cyclic aromatic hydrocarbons (PAH), phenols, and benzene compounds) and aliphatic compounds containing esters, alkynes, olefins, and acids, as presented in Fig. 4f. With the increase of N-doped Fe loading, the phenolic compounds in the aromatic compounds increased continuously from 28.40 area.% to 76.90 area.% and the aliphatic compounds decreased from 20.05 area.% to 2.33 area.%. It indicated that phenolic compounds show significant selectivity with increasing metallic component loading. The loading of N-doped Fe accelerated the inverse alkene reaction, and Maccoll elimination reaction in pyrolysis, and the positive electronegativity of Fe could attract the negatively charged methyl and aldehyde groups in the side chains of the compounds, which promoted the generation of phenolic compounds in bio-oil [34].

The phenolic compounds in lignin bio-oil are classified into nine main species. As illustrated in Fig. 4g, the phenol selectivity rises from 15.28 % to 46.20 % with increasing metallic component loading, which is higher than that of compounds such as cresol and proxmethylphenol. It indicates that the loading of metallic components facilitates the demethylation of phenol derivatives to form phenol. The significant decrease in the selectivity of the three compounds containing multiple methyl and methoxy side chains in Fig. 4h. It is owing to the cleavage of the lignin cross-linked structure into a large number of aromatic hydrocarbons during pyrolysis. The side-chain groups of these compounds break under the addition of Fe-N₂₅/HZSM-5 to produce phenolic compounds, such as phenol, containing few side chain.

3.2.2. Catalyst characterization after reaction

In order to analyze the changes in the surface groups of the catalyst during pyrolysis, the catalyst was characterized by FTIR after the reaction. As illustrated in Fig. 5a, the peak around 3400 cm⁻¹ is attributed to the hydroxyl (–OH) stretching vibration of HZSM-5, and its peak area increases with the loading of the metallic component, suggesting that the increase of N-doped Fe loading is favorable to the retention and formation of the –OH structure during the lignin pyrolysis [35]. The

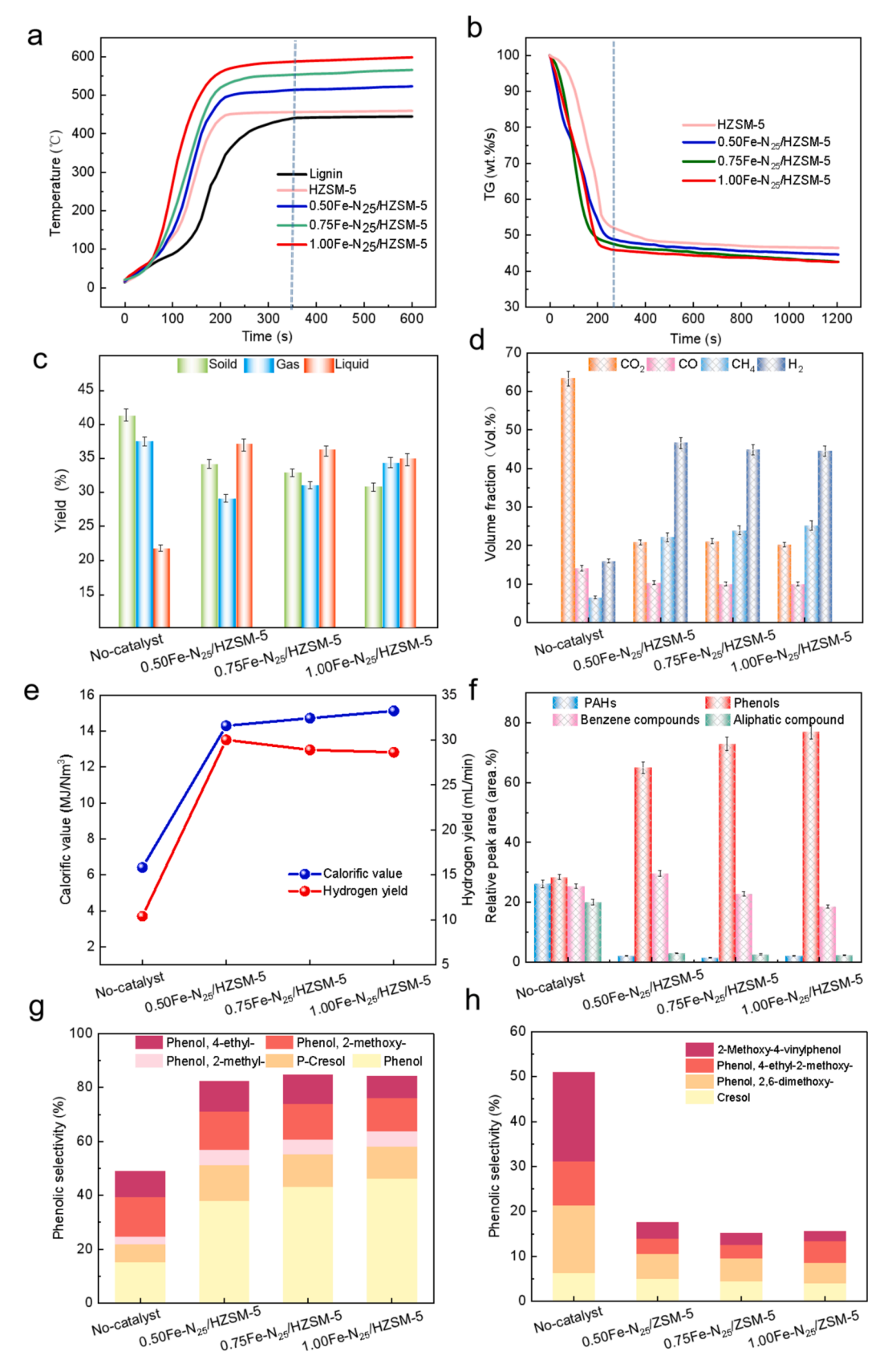
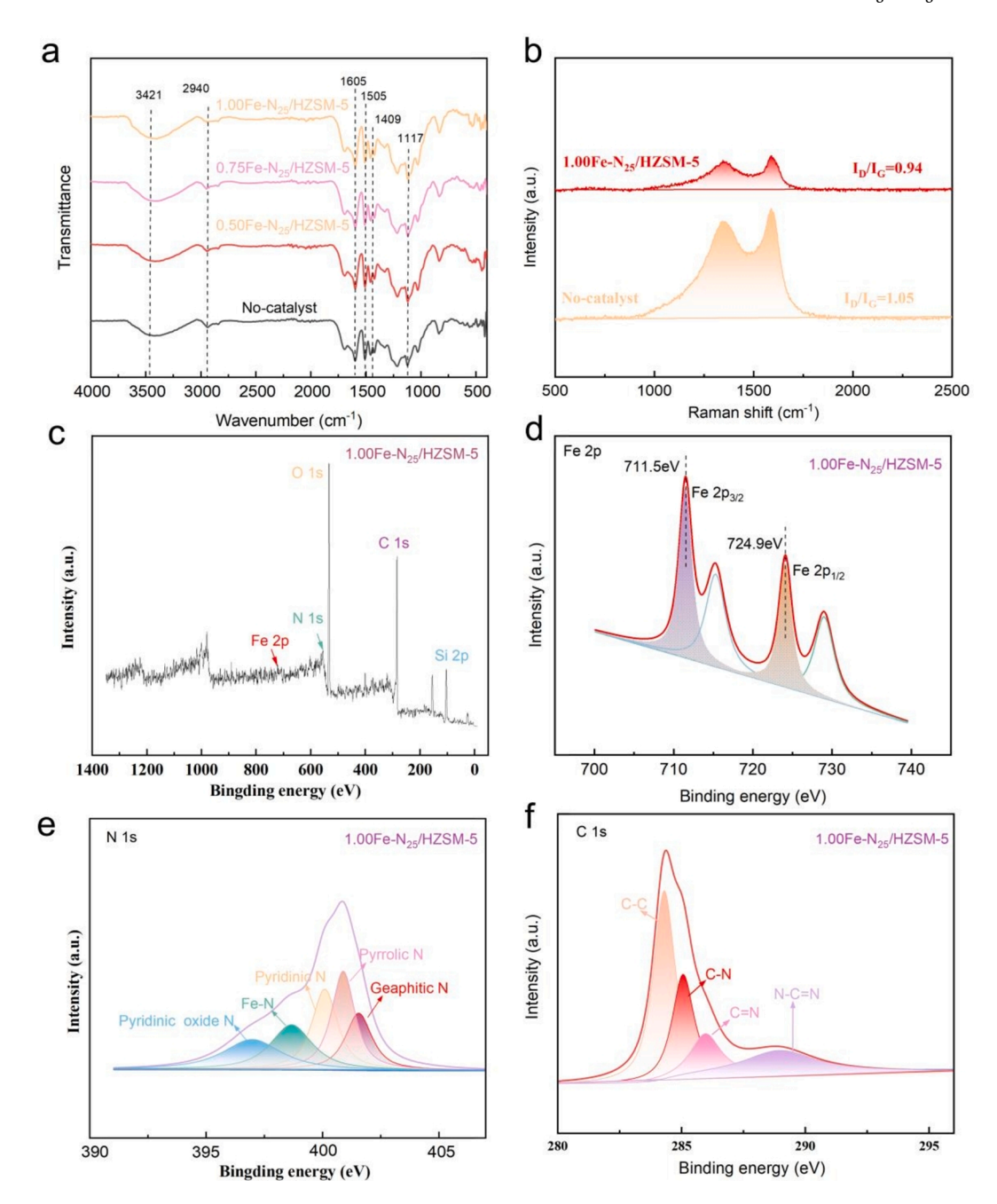


Fig. 4. Thermal decomposition heating characteristics and product distribution. a. Temperature rise curve; b. TG; c. Product yield; d. Bio-gas composition; e. Calorific value and hydrogen production rate; f-g. Bio-oil selectivity.



 $\textbf{Fig. 5. Characterization of catalysts after the reaction.} \ a. \ FTIR; \ b. \ Raman; \ c-f. \ XPS.$

peaks at 1459 cm⁻¹, 1505 cm⁻¹, and 1605 cm⁻¹ are attributed to lignin's aromatic backbone vibration and C-O stretching vibration. The peaks increase in proportion with the increase of metallic components loading, indicating benzene ring structure formation in pyrolyzed carbon. Raman analysis of the reacted catalyst is illustrated in Fig. 5b. Both the D and G peaks are clearly visible, and the intensity ratio (I_D/I_G) of the D and G bands reflects the degree of graphitization and disorder of the catalyst. The 1.00Fe- N_{25} /HZSM-5 catalyst was discovered to have an I_D / I_G value of 0.94, indicating that the degree of structural defects and graphitization was significant, which was more conducive to the adsorption of lignin and the desorption of the products during the pyrolysis [30]. In order to analyze the chemical composition and valence states of the catalyst after the reaction, XPS characterization of 1.00Fe-N₂₅/HZSM-5 was carried out, as illustrated in Fig. 5c, d, e, and f. It was found that the peak at 719.2 eV in the high-resolution energy spectrum of Fe 2p disappeared, while the peaks of Fe-N corresponding to 711.5 eV

and 724.9 eV increased, which suggested that the metal fractions loaded on HZSM-5 retained a good chemical morphology after pyrolysis. The four typical N-C structures in the N 1s high-resolution energy spectrum are consistent with those on the fresh catalysts, among which the Fe-N peak are enhanced. This indicates that the abundant acidic sites of HZSM-5 provide anchor sites for the metal components, which inhibit the redox reaction of Fe in the pyrolysis reaction and improve the stability of the metal components in the pyrolysis [36]. The four peaks in the C 1s spectrum are N-C = N (298.1 eV), C = N (286.3 eV), C-N (284.7 eV), and C-C (284.2 eV), which are the same as the high-resolution energy spectra of C1s before pyrolysis but with reduced peak areas, indicating that a small portion of elemental N is doped into the graphitic carbon network in pyrolysis to form a different N-C structure [30].

3.2.3. Catalyst stability test

The catalysts used was treated by complete ultrasonic washing, and

then it was filtrated and calcined at a microwave oven. The catalyst was regenerated by the above processing. To ensure that the coke deposited on the catalyst's surface are almost removed. The catalyst of Fe-N $_{25}/$ HZSM-5 was chosen to perform the stability test. The stability test was conducted by three and five cycles at the microwave power of 700 W, with duration of 30 min for one cycle, respectively. The distribution of pyrolysis products and the composition of gaseous products after different cycles were analyzed, and also the used catalysts after different cycles were characterized by XPS and XRD, as displayed in Fig. 6.

As can be seen from Fig. 6a, the bio-oil yield reduced and meanwhile the bio-char yield increased to some extent with the increase of cycles. Despite this, the actual change was relatively low after five cycles, respectively with the changing amplitude of 6.2 % for bio-char and 8.5 % for bio-oil. For the bio-gas yield, there was no visible changes after different cycles, maintaining at around 33.8 wt%. The results in Fig. 6b further revealed that the main compositions in the bio-gas were almost unchanged after different cycles. These results show that Fe-N25/HZSM-5 exhibits the favorable stability in process of the microwave catalytic pyrolysis of lignin. This meanwhile reflects the cokes generated in the pyrolysis process are effectively removed by the regeneration process. It was found from the XPS characterization results (Fig. 6c) that there was no much noticeable changes on the intensities of Fe $2p_{3/2}$ and Fe $2p_{1/2}$ in the high-resolution energy spectrum of Fe-N25/HZSM-5 after different cycles. After three and five cycles, the characteristic peaks of HZSM-5 pore periodicity and high crystallization at the range of $12.0^{\circ} \sim 18.0^{\circ}$ and $22.5^{\circ} \sim 37.0^{\circ}$ were still observed on the XRD spectra of Fe-N₂₅/ HZSM-5, as shown in Fig. 6d. Both XPS and XRD analysis results point that the N-doped Fe can still maintain well dispersion after several cycles, without destroying the MFI topography of HZSM-5. This is the internal cause to favorable stability of Fe-N $_{25}$ /HZSM-5 in process of the microwave catalytic pyrolysis of lignin.

3.2.4. Potential of microwave catalytic pyrolysis of lignin First of all, the N-doped Fe supported on HZSM-5 is proved to have

favorable catalytic effect on microwave pyrolysis of lignin, increasing the hydrogen production and improving the selectivity of phenolic compound in the bio-oil. From the perspective of the pyrolysis products, the technology of microwave catalytic pyrolysis of lignin over HZSM-5 supported with N-doped Fe has great economic potential for the high-value utilization of lignin as well as the other biomass resources, which can greatly increase the value of pyrolysis products.

Secondly, the catalyst of N-doped Fe supported on HZSM-5 presents a desirable stability. This is because that microwave irradiation is efficient to remove the carbon deposited on the catalyst surface in the regeneration process. The excellent catalyst stability is conducive to improve the utilization efficiency and reduce preparation costs of the catalyst, showing potential for sustainable utilization of the catalyst.

Last but no least, Fe is a common and green active component for the catalyst preparation, with abundant resource and low cost. Besides, the treatment of N-doping on Fe and the regeneration of the used catalyst are easy to be performed. Overall, the work offers a simple method for the catalyst preparation and regeneration, also highlighting the application potential of the technology.

3.3. Possible pathways of lignin pyrolysis

Guaiacol was chosen as a lignin model because its molecule contains key hydroxyl (C_1 -OH) and methoxy (C_6 -OCH₃) groups. The increase of phenolic compounds in pyrolysis oils is derived from the breakage of these side chain groups [37]. Therefore, guaiacol was optimized based on GaussView 5.0 and Gaussian 09 W, using the density functional theory method (DFT), including calculations of adsorption of guaiacol by N-doped metallic components and Fe-N₂₅/HZSM-5, respectively.

3.3.1. Adsorption of guaiacol by N-doped metallic components

Considering element N forms species such as pyridine nitrogen, pyrrole nitrogen and graphite nitrogen in graphitic carbon networks, different nitrogen-carbon species with or without metal embedding are

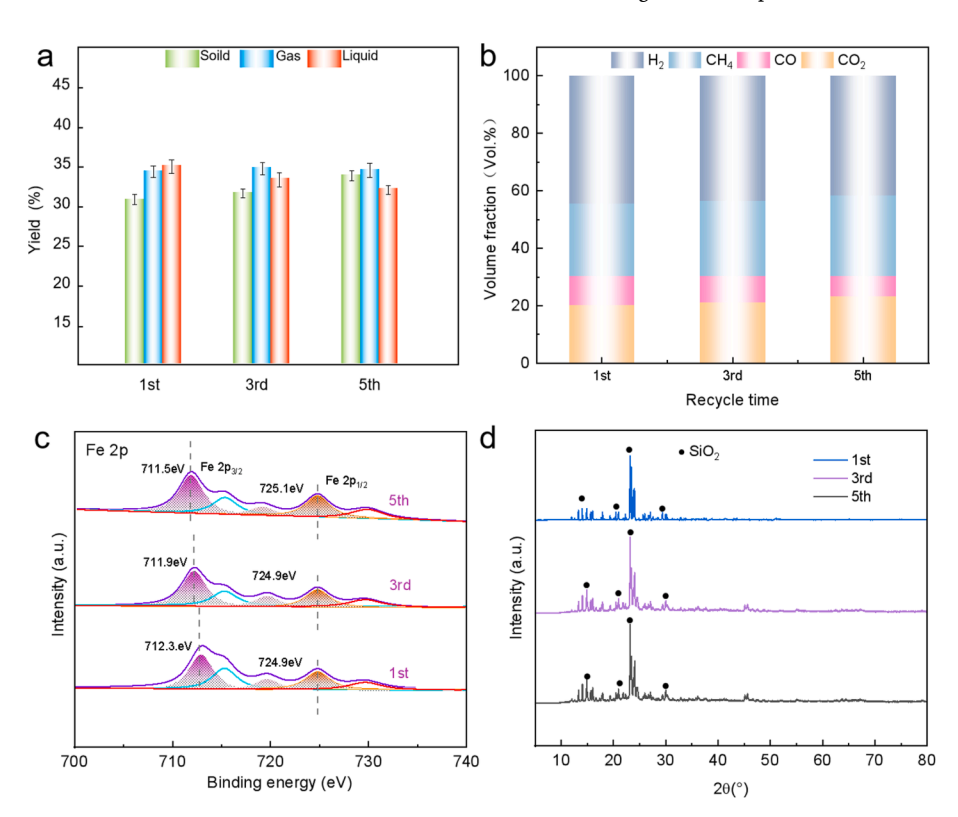


Fig. 6. Stability test and characterization on the catalyst after different cycles. a. Pyrolysis products distribution; b. bio-gases composition; c. XPS analysis; d. XRD analysis.

used as adsorption substrates to figure out their effects on the adsorption of guaiacol. Fig. 7a and Fig. 7b illustrate the trends of key bond lengths and adsorption spacing of the guaiacol after adsorption on the eight substrates: Grap-C, Grap-N, Pyri-N, Pyrr-N, Fe-Pyri-N, Co-Pyri-N, Fe-Pyrr-N and Co-Pyrr-N. Adsorption on Fe-Pyrr-N increased the C1-OH bond length to 1.374 Å. The adsorption of Fe-Pyri-N did not change the C₁-OH bond length significantly but enhanced the C₆-OCH₃ and O-CH₃ bond lengths to 1.396 and 1.439 Å, respectively. This indicates that after loading of N-doped metallic components, the substrate forms coordination bonds with the metal, enhancing the adsorption of the guaiacol. In contrast, the O-CH₃ and C₆-OCH₃ bond lengths did not change much after the adsorption of the guaiacol with Co-Pyri-N and Co-Pyrr-N. This observation suggests that the activity of Co is lower than that of Fe. C₁-OH and C₆-OCH₃ were analyzed with the O atoms of C₁-OH and C₆-OCH₃ as fixed sites, and it was found that C₁-OH preferred to adsorb to the N atoms, while C₆-OCH₃ preferred to adsorb to metal sites. This leads us to believe that doping of the metallic components leads to an increase in the length of the side-chain groups and linkage bonds in the moldings,

causing a decrease in the bond energy and easier breakage.

The analysis of changes in structural bond lengths can reveal changes in molecular conformation and bond-breaking features. In contrast, the analysis of energy changes can be found in the thermodynamic properties and catalytic activity of the reaction system. Fig. 7c shows the changes in free energy, enthalpy, internal energy and electron energy after the adsorption of eight substrates. All the system's thermodynamic parameters decreased after the substrate's absorption, with the most obvious changes in Fe-Pyrr-N. Fig. 7d shows the adsorption energy and enthalpy difference curves after the adsorption of guaiacol on eight substrates. The adsorption energies of the guaiacol on the substrate were all negative, and the adsorption energies were all significantly reduced after the metallic components were N-doped. It indicated that N-doped metallic components adsorption of guaiacol was more stable, while the lower energy gap and higher reactivity of Fe-Pyrr-N made the adsorption more likely to occur. This was also evident by the enthalpy changes, where the enthalpy differences for all substrates except Grap-N were negative. After the adsorption of guaiacol on Fe-Pyrr-N, the enthalpy

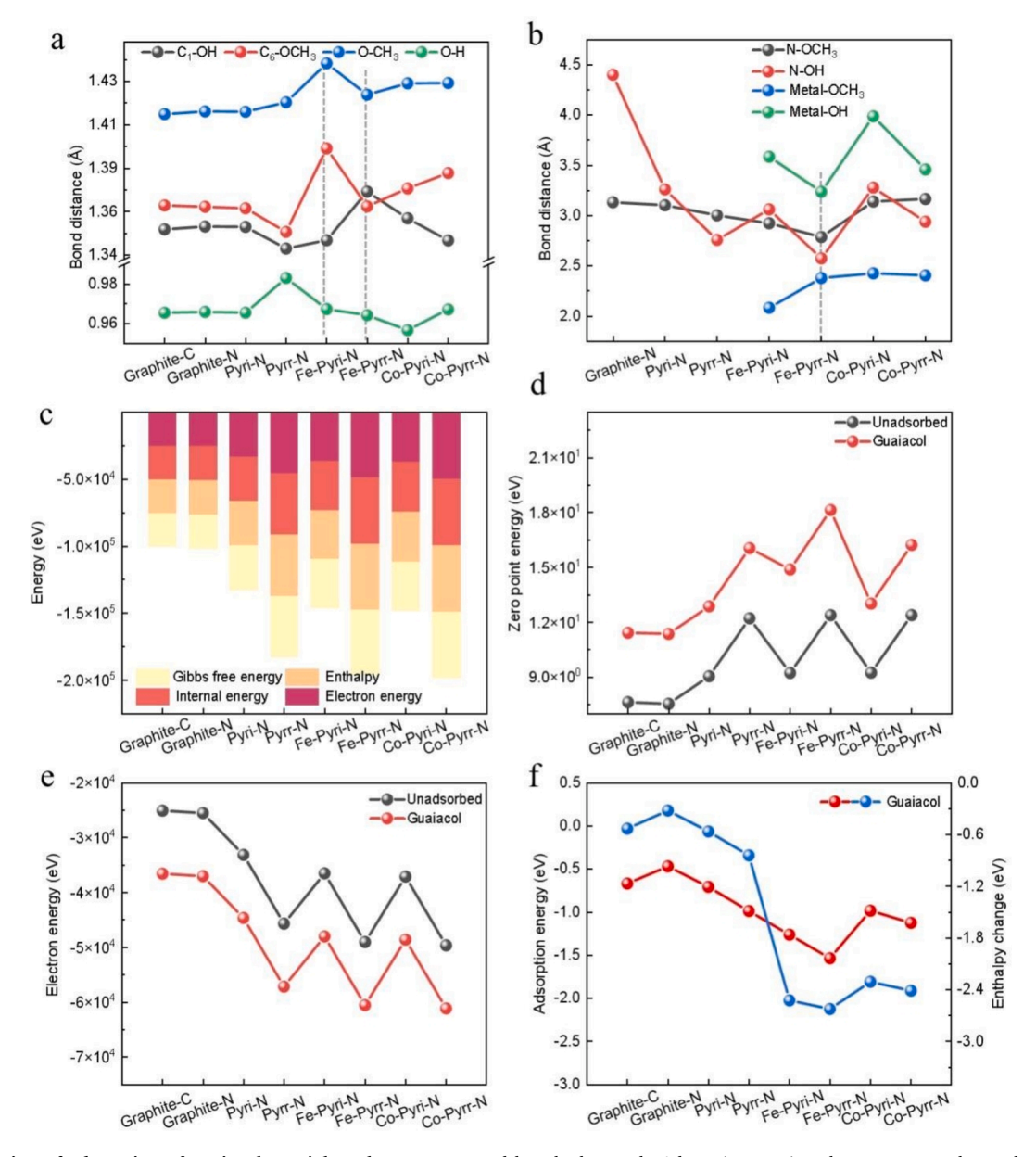


Fig. 7. Calculation of adsorption of guaiacol on eight substrates. a. Bond length change; b. Adsorption spacing change; c. Four thermodynamic parameter change; d. Adsorption energy and enthalpy difference.

difference was -2.621 eV, making it easier to form the adsorption state. This suggested that the substrate Fe-Pyrr-N was the main reason for the nitrogen-doped metal component to enhance the catalytic activity of HZSM-5, which was the same as the results of the previous analyses.

3.3.2. Adsorption of guaiacol by Fe-N₂₅/HZSM-5

HZSM-5 5 T (5 T) and HZSM-5 8 T (8 T) were chosen as substrates in order to more accurately describe the acid sites at straight and sinusoidal pores and cross cavities of the molecular sieve MFI topology [38]. On this basis, HZSM-5 8 T loaded clusters(8 T loaded) were used to represent the loaded molecular sieve model to reduce the computational effort. In order to ensure the balance of positive and negative charges in the model to ensure the accuracy of the calculations, N-doped metallic components were Fe-N complex for loading. The blue region (-8.774×10^{-2} eV) on the silica-alumina-oxygen skeleton of the 5 T model in Fig. 8a is a straight string aperture, representing the Lewis acidic site of HZSM-5. The model of 8 T contains acid-base sites in straight and sinusoidal apertures, with the red region (3.749×10^{-2} eV) and the blue region (-3.749×10^{-2} eV) corresponding to the basic and acidic sites in HZSM-5. The yellow region (3.055×10^{-2} eV) on the N atom indicates

the electron cloud's new positive density distribution after loading the Fe-N complex. The electrostatic interaction between the N-doped metallic components and the positively charged HZSM-5 occupies the cavities on the catalyst's surface. Meanwhile, the two new strong acidic sites appeared as dark blue regions ($-5.864\times10^{-2}\mathrm{eV}$), suggesting that the 8 T loaded model van der Waals surface electrostatic potential (ESP) exhibited stronger potentiometric values compared to the 8 T model. The energy gap structure of 8 T is seen to be smaller compared to 5 T in Fig. 8b, and the energy gap of the 8 T loaded model is 0.12 eV, which is 55.86 % lower than that of 8 T. This again proves that the loading of the N-doped metallic components increases the catalytic acidic site of the molecular sieve and improves the catalytic activity of the catalyst.

As illustrated in Fig. 8c, the C_1 -OH, O-H, and C_6 -OCH₃ bond lengths increased to 1.370 Å, 0.980 Å, and 1.401 Å, respectively, after adsorption of guaiacol on Fe-N/HZSM-5 8 T, which showed the changes of bond lengths were the most evident on this model. It is calculated that for models 5 T and 8 T, the acidity of the sinusoidal pores in the HZSM-5 structure is higher than that of the rectilinear pores, which is more conducive to weakening the bonding energy of the monomer side chain structure. Fig. 8d reflects the changes in free energy, enthalpy, internal

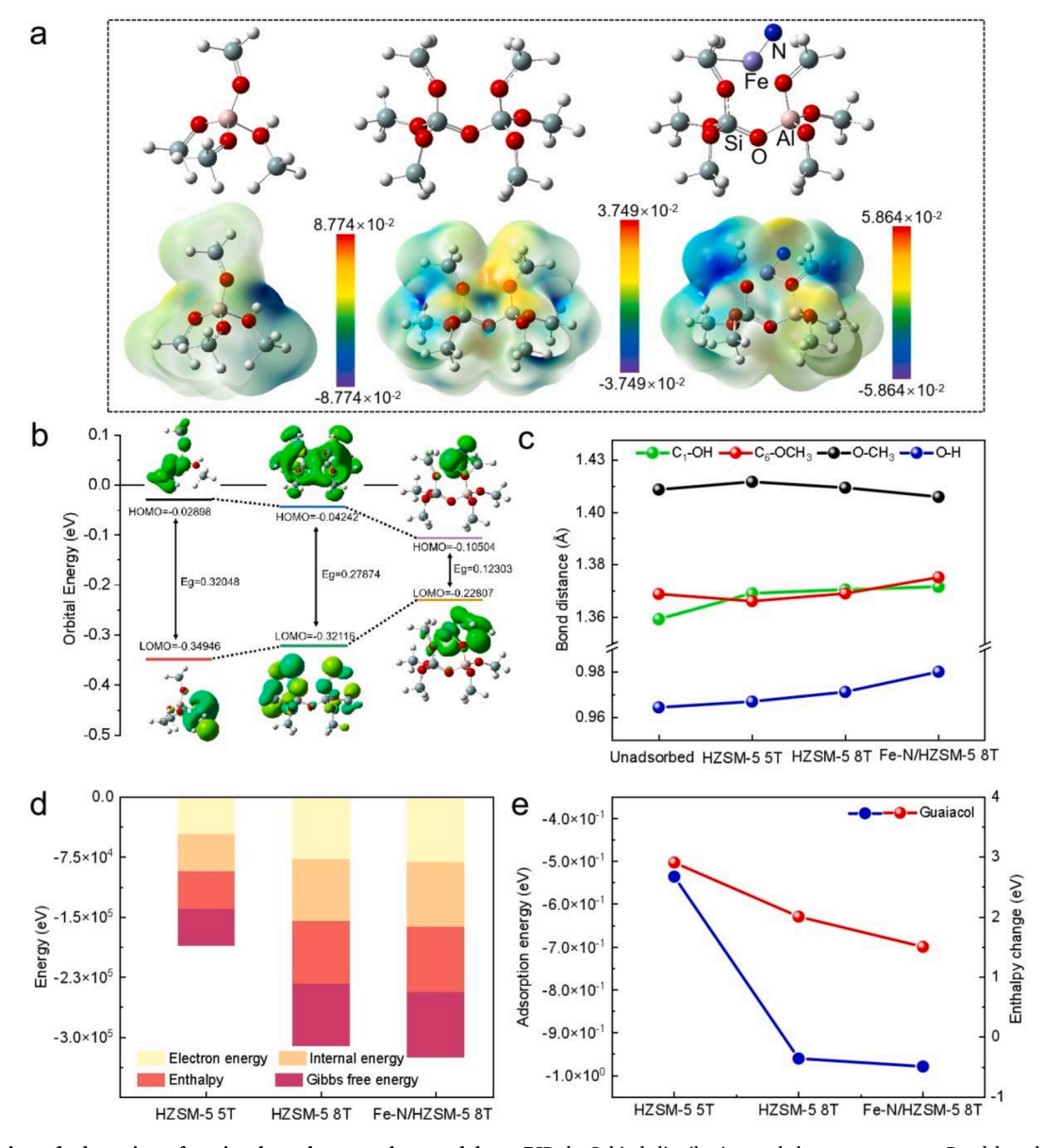


Fig. 8. Calculation of adsorption of guaiacol on three catalyst models. a. ESP; b. Orbital distribution and the energy gap; c. Bond length change; d. Four thermodynamic parameter change; e. Adsorption energy and enthalpy difference.

energy and electron energy under the adsorption of guaiacol on different catalyst models. Each thermodynamic eigenvalue is the highest for the 5 T and the lowest for the 8 T loading model. It indicated that N-doped Fe can produce weak interaction forces with the skeleton of molecular sieves, leading to high catalyst activity after loading. In contrast, the significant reduction in electron energy is because of the intramolecular interactions, such as ESP, under the absorption of guaiacol on different catalyst models, resulting in lower total energy and a more stable system. The above comparison of the three HZSM-5 models reveals the largest change in critical bond length and greater stability after the absorption of guaiacol on the 8 T loaded model.

To further illustrate the stability of the catalyst after adsorption, the adsorption energies and enthalpy differences of guaiacol on difference catalyst models are depicted in Fig. 8e. The adsorption energies of guaiacol on different catalyst models were all negative, and the 8 T loaded model had the smallest adsorption energy, suggesting that the loading of nitrogen-doped metal components made it easier for HZSM-5 to adsorb lignin. Further analysis of the enthalpy difference revealed that the 8 T loaded model had the smallest enthalpy difference relative to the unloaded model. This meant the reaction was more exothermic and favourable to lignin pyrolysis. In conclusion, the loading of N-doped Fe increased the acidic site of HZSM-5, which resulted in higher adsorption stability of guaiacol on the loaded catalyst model, and improving the activity of Fe-N₂₅/HZSM-5. This finding was consistent with previous analyses and contributed to microwave catalytic pyrolysis of lignin.

3.3.3. Calculation of cleavage pathways of lignin modelling compounds

Significant stretching of the C_1 -OH and C_6 -OCH $_3$ bond lengths occurred after the adsorption of guaiacol over the Fe-N loaded HZSM-5 8 T catalyst and the adsorption spacing to the catalyst active site tended to be close, suggesting that the bond breaking of guaiacol is most likely to occur on the side-chain moiety. Based on this, three possible pathways were proposed, and the energy trends of the three pathways were simulated using DFT to find the optimal pyrolysis pathway, as indicated in Fig. 9.

Hydrogen radicals generated by lignin pyrolysis have a nonnegligible role in the cleavage of the modal molecules and the formation of the products so that the introduction of exogenous hydrogen radicals can better fit the pyrolysis process of guaiacol. The energy barrier of TS1 in pathway 1 is 0.14 eV, and the reaction energy is -0.1eV for breaking the methoxy group into phenol and ethanol under the hydrogen radical, suggesting that the rate determining step is TS1. The energy barrier of the TS2 in pathway 2 is 0.2 eV. Pointing to the fact that the hydrogen radical undergoes a protonation reaction to produce the intermediate methylphenol and water, followed by adsorption of the intermediate with the hydrogen radical, reducing the adsorption energy to 2.35 eV. The TS3 in pathway 2 has an energy barrier of 0.12 eV. This finding suggests that the methyl oxygen of the intermediate is removed by down-binding with the hydrogen radical, resulting in the formation of phenol and methane. Since the energy barrier of TS2 is higher than that of TS3, the adsorption energy is reduced to -0.03 eV, suggesting that TS2 is the rate-determining step of pathway 2. Pathway 3 has an energy barrier of 0.29 eV for TS4, at which point the methyl group in guaiacol breaks and hydrogenates to produce a catechol intermediate

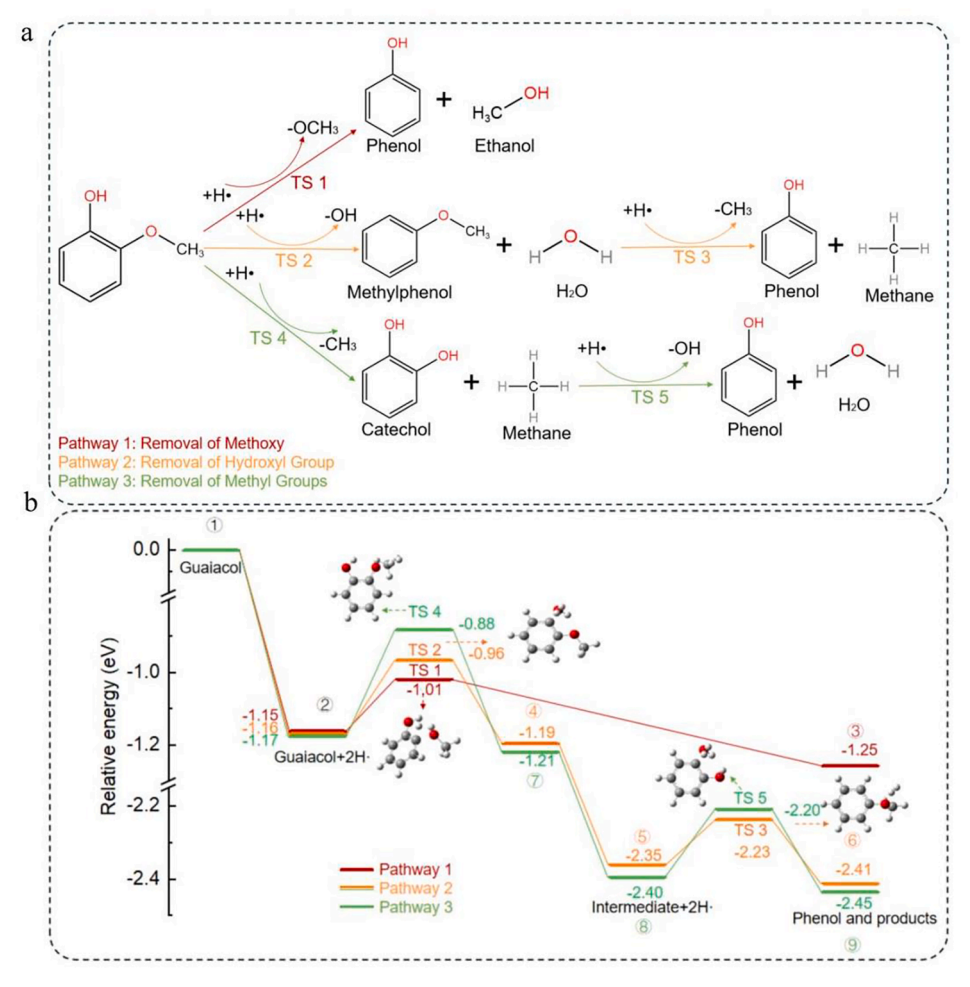


Fig. 9. Possible pathways and energy barriers. a. Proposed reaction path; b. Energy barriers.

with methane. The adsorption energy was reduced by 2.40 eV after the introduction of hydrogen radicals, followed by the decomposition of the intermediate to phenol and water through TS5 in a dehydration reaction. The decrease in adsorption energy to -0.04 eV suggests that the decisive step in pathway 3 is TS4. In summary, the activation energy barrier required for the rate-determining step in pathway 1 is significantly lower than that of pathway 2 and pathway 3. This reveals that pathway 1 is the optimal pathway for the conversion of guaiacol into phenol, which is kinetically more favourable to occur. In agreement with the analytical results in Fig. 4g, the bio-oil is transformed into phenolic compounds, and the phenol selectivity is up to 46.20 % in the presence of 1.00 Fe-N $_{\rm 25}/\rm HZSM$ -5.

4. Conclusions

In this work, HZSM-5 supported with N-doped Fe was applied to the microwave catalytic pyrolysis of lignin. The experimental and simulation results demonstrated the loading of N-doped Fe on the HZSM-5 increased the catalyst's acidity, achieving high activity and stability. With the use of the catalyst, the selectivity of phenolic compounds in the bio-oil reached 76.90 % and the content of $\rm H_2$ in the bio-gas was up to 44.54 vol%. The calculation using DFT method on a model compound (guaiacol) further elucidated intrinsic role of the N-doped Fe on the microwave catalytic pyrolysis of lignin, which indicated the Fe-Pyrr-N adsorption not only greatly changed the bonds length of model compound but also made them more stable.

CRediT authorship contribution statement

Yan Wang: Writing – original draft. Kangqi Cao: Supervision. Wenlong Sun: Investigation. Xiangxi Lin: Investigation. Jianwei Wang: Methodology. Jessica Villarreal: Writing – review & editing. Longzhi Li: Writing – review & editing.

Declaration of competing interest

The authors declare that they have no known competing financial interests or personal relationships that could have appeared to influence the work reported in this paper.

Acknowledgements

This work has been supported by National Natural Science Foundation of China (No. 22172091), China Postdoctoral Science Foundation (No. 2019M652432), Natural Science Foundation of Shandong Province (ZR2021ME184).

Data availability

No data was used for the research described in the article.

References

- P.L. Sun, Z.D. Wang, C.Z. Li, et al., Catalytic conversion of lignin and its derivatives to alkanes over multifunctional catalysts: a review, Fuel 361 (2024) 130726.
- [2] Q.Q. Liu, L. Luo, L.Q. Zheng, Lignins: biosynthesis and biological functions in plants, Int. J. Mol. Sci. 19 (2018) 335.
- [3] J. Sternberg, O. Sequerth, S. Pilla, Green chemistry design in polymers derived from lignin: review and perspective, Prog. Polym. Sci. 113 (2021) 101344.
- [4] N.L. Radhika, S. Sachdeva, M. Kumar, Lignin depolymerization and biotransformation to industrially important chemicals/biofuels, Fuel 312 (2022) 122935.
- [5] P. Sirous-Rezaei, Y.K. Park, Catalytic hydropyrolysis of lignin: suppression of coke formation in mild hydrodeoxygenation of lignin-derived phenolics, Chem. Eng. J. 386 (2020) 121348.
- [6] D. Duan, R. Ruan, Y. Wang, et al., Microwave-assisted acid pretreatment of alkali lignin: effect on characteristics and pyrolysis behavio, Bioresour. Technol. 251 (2018) 57–62.

- [7] L. Li, K. Cao, D. Cai, et al., Influences of iron additives on microwave-assisted pyrolysis of woody biomass and microwave-induced discharge with spherical biochar, Energy 276 (2023) 127549.
- [8] L. He, Y. Ma, C. Yue, et al., The heating performance and kinetic behaviour of oil shale during microwave pyrolysis, Energy 244 (2022) 123021.
- [9] A. Zaker, Z. Chen, X. Wang, et al., Microwave-assisted pyrolysis of sewage sludge: a review, Fuel Process. Technol. 187 (2019) 84–104.
- [10] Q. Bu, H. Lei, S. Ren, et al., Production of phenols and biofuels by catalytic microwave pyrolysis of lignocellulosic biomass, Bioresour. Technol. 108 (2012) 274–279.
- [11] S. Farag, B.P. Mudraboyina, P.G. Jessop, et al., Impact of the heating mechanism on the yield and composition of bio-oil from pyrolysis of kraft lignin, Biomass Bioenergy 95 (2016) 344–353.
- [12] Q. Xie, S. Li, R. Gong, et al., Microwave-assisted catalytic dehydration of glycerol for sustainable production of acrolein over a microwave absorbing catalyst, Appl. Catal. B 243 (2019) 455–462.
- [13] Y. Liu, C. Zhou, A.A. Siyal, et al., Comparative microwave catalytic pyrolysis of cellulose and lignin in nitrogen and carbon dioxide atmospheres, J. Clean. Prod. 437 (2024) 140750.
- [14] R. Kupila, K. Lappalainen, T. Hu, et al., Lignin-based activated carbon-supported metal oxide catalysts in lactic acid production from glucose, Appl. Catal. A 612 (2021) 118011.
- [15] X. Li, G. Chen, C. Liu, et al., Hydrodeoxygenation of lignin-derived bio-oil using molecular sieves supported metal catalysts: a critical review, Renew. Sustain. Energy Rev. 71 (2017) 296–308.
- [16] D. Yang, J. Huang, Z. Hu, et al., Catalytic pyrolysis of lignin to aromatic hydrocarbons over Nb/Al catalyst, Energy (2024) 131764.
- [17] A. Hendry, M. Åhlén, T. Fernandes, et al., Catalytic cracking of Etek lignin with zirconia supported metal-oxides for alkyl and alkoxy phenols recovery, Bioresour. Technol. 317 (2020) 124008.
- [18] M. Huang, Z. Ma, B. Zhou, et al., Enhancement of the production of bio-aromatics from renewable lignin by combined approach of torrefaction deoxygenation pretreatment and shape selective catalytic fast pyrolysis using metal modified zeolites, Bioresour. Technol. 301 (2020) 122754.
- [19] W. Gao, X. Tang, H. Yi, et al., Mesoporous molecular sieve-based materials for catalytic oxidation of VOC: a review, J. Environ. Sci. 125 (2023) 112–134.
- [20] I. Kurnia, S. Karnjanakom, A. Bayu, et al., In-situ catalytic upgrading of bio-oil derived from fast pyrolysis of lignin over high aluminum zeolites, Fuel Process. Technol. 167 (2017) 730–737.
- [21] Q. Zou, H. He, J. Xie, et al., Study on the mechanism of acid modified H-Beta zeolite acidic sites on the catalytic pyrolysis of Kraft lignin, Chem. Eng. J. 462 (2023) 142029.
- [22] M. Shamzhy, M. Opanasenko, P. Concepción, et al., New trends in tailoring active sites in zeolite-based catalysts, Chem. Soc. Rev. 48 (4) (2019) 1095–1149.
- [23] H. Liu, H. Liu, J. Hu, et al., Comprehensive study of alkali lignin pyrolysis catalyzed by composite metal-modified molecular sieves for the preparation of hydrocarbon liquid fuels, J. Anal. Appl. Pyrol. (2024) 106608.
- [24] S. Chen, R. Wojcieszak, F. Dumeignil, et al., How catalysts and experimental conditions determine the selective hydroconversion of furfural and 5hydroxymethylfurfural, Chem. Rev. 118 (22) (2018) 11023–11117.
- [25] B. Lu, Q. Liu, S. Chen, Electrocatalysis of single-atom sites: impacts of atomic coordination, ACS Catal. 10 (14) (2020) 7584–7618.
- [26] J. Li, S. Ma, R. Cui, et al., Study on the mechanism of catalytic oxidation of NO with H₂O₂ based on fly-ash-derived Fe/ZSM-5 catalysts, Energy Fuel 36 (12) (2022) 6397–6408
- [27] X. Gao, Y. Zhou, S. Liu, et al., Single cobalt atom anchored on N-doped graphyne for boosting the overall water splitting, Appl. Surf. Sci. 502 (2020) 144155.
- [28] X. Yang, R. Zhou, G. Liu, et al., Reduce energy consumption for organic amine regeneration by MnOOH/HZSM-5 catalysts, Chem. Eng. J. (2024) 152564.
- [29] Y. Xu, H. Tang, L. Liu, et al., Hierarchical Fe/ZSM-5 zeolites for efficient Hg0 removal from coal-fired flue gas, Chem. Eng. J. 450 (2022) 138180.
- [30] X. Wu, H. Li, F. Ge, et al., N-doped MOF-lignin hybrid catalyst for highly selective hydrodeoxygenation of lignin-derived phenols, Chem. Eng. J. (2024) 153009.
- [31] F. Cao, Q. Zhao, D. Kong, et al., Turning the coordination environment of atomic Fe-N₄ center by peripheral nitrogen species for boosted catalytic performance, Chem. Eng. J. 473 (2023) 145181.
- [32] T. Jin, H. Wang, J. Peng, et al., Catalytic pyrolysis of lignin with metal-modified HZSM-5 as catalysts for monocyclic aromatic hydrocarbons production, Fuel Process. Technol. 230 (2022) 107201.
- [33] Y. Wang, Y. Zhang, Y. Gao, et al., Modulating Lewis acidic active sites of Fe doped Bi₂MoO₆ nanosheets for enhanced electrochemical nitrogen fixation, J. Colloid Interface Sci. 646 (2023) 176–184.
- [34] A.T. To, D.E. Resasco, Hydride transfer between a phenolic surface pool and reactant paraffins in the catalytic cracking of m-cresol/hexanes mixtures over an HY zeolite, J. Catal. 329 (2015) 57–68.
- [35] H. Zhang, B. Luo, K. Wu, et al., Ex-situ catalytic pyrolysis of lignin using lignincarbon catalyst combined with HZSM-5 to improve the yield of high-quality liquid fuels, Fuel 318 (2022) 123635.

- [36] X. Guo, J. Yin, S. Xia, et al., A novel bifunctional catalyst obtained by in situ introduction of hierarchically structured HZSM-5 for direct DME synthesis from CO₂ hydrogenation, Fuel 364 (2024) 131057.
 [37] F. Ge, H.H. Xia, J. Li, et al., Lignin meets MOFs: lignin derived metal carbon
- [37] F. Ge, H.H. Xia, J. Li, et al., Lignin meets MOFs: lignin derived metal carbon material for the catalytic hydrotreatment of guaiacol to cyclohexanol, Chem. Eng. J. 473 (2023) 145375.
- [38] Y. Horbatenko, J.P. Pérez, P. Hernandez, et al., Reaction mechanisms for the formation of mono-and dipropylene glycol from the propylene oxide hydrolysis over ZSM-5 zeolite, J. Phys. Chem. C 118 (38) (2014) 21952–21962.